Interface dynamics and solute trapping in alloy solidification with density change

Massimo Conti and Marco Fermani
Dipartimento di Fisica, Universitá di Camerino, and Istituto Nazionale di Fisica della Materia, Via Madonna delle Carceri, I-62032 Camerino, Italy
(Received 8 July 2002; published 21 February 2003)

We present a phase-field model for the solidification of a binary alloy, which incorporates hydrodynamic effects due to the different densities of the solid and liquid phases. We start from a generalized thermodynamic potential with squared gradient terms for the associated fields; the condition of local positive entropy production is then utilized to derive a set of equations that drive the system towards equilibrium. The model has been numerically solved in one dimension, to investigate the effects of the flow field on the interface dynamics. We observed that solute trapping is almost unaffected by the fluid advection, while the interface mobility is strongly reduced as the fluid velocity increases. This reflects on the dependence of the interface temperature T_I on the growth rate v_I: the region of the unstable (ascending) branch is reduced, and the maximum of the $T_I(v_I)$ curve is shifted towards lower velocities.

DOI: 10.1103/PhysRevE.67.026117 PACS number(s): 05.70.Fh, 81.10.Mx, 64.70.Dv, 05.70.Ln

I. INTRODUCTION

The growth of a crystal from the melt is a complex phenomenon that involves many physical effects. The rejection of the latent heat (and solute, for alloy solidification), away from the solid-liquid interface, is accompanied by the formation of thermal and solute boundary layers which strongly affect the morphological instability of the interface. Moreover, across the interface the density changes (the solid is generally denser than the liquid); the change ranges from a few percent for simple metals to more than 20% for some eutectic mixtures. The shrinking, or in some cases the dilatation, of the system causes an advection flow in the liquid phase. Then, even in absence of gravity, the purely diffusive picture for the conserved fields in the bulk phases should be extended, to incorporate hydrodynamic effects. Recently, this subject attracted an increased attention for practical reasons. The reduction in volume in metal solidification is a source of stress at the growing interface, and may induce cavitation, with formation of defects or micropores in cast products [1,2]. A further effect results from the dynamic pressure drop across the melt: at large growth rates, the change of the melting temperature with pressure may significantly alter the undercooling of the liquid phase.

Hydrodynamic effects in solidification far from equilibrium have been previously considered by Horvay [3] for a pure material. Using a free-boundary approach, he studied the growth of a spherical nucleus into an undercooled melt of lower density. The liquid phase was treated as an incompressible inviscid fluid with a transition temperature affected by both the curvature of the nucleus and the hydrodynamic pressure due to the flow. The numerical solution of this model led Horvay to conclude that at large undercooling the tension field at the interface could induce a change in the microstructure of the solid. A similar analysis was subsequently conducted by Charach and Rubinstein [4] for the growth of a planar interface. These authors showed that, due to the effects of the pressure field, some inconsistencies of the Stefan formulation of the problem could be removed and the interface velocity is free of singularities during the entire freezing process.

The above studies were based on the notion of a sharp interface separating the two phases; the governing equations of the model express the conservation of mass, momentum, and energy in each of the bulk phases, with proper interface boundary conditions. With respect to the original Stefan problem, the latter must incorporate additional constraints for the mass and momentum conservation.

A more recent approach to the density effects in solidification is based on the diffuse interface picture, through an extension of the phase-field model. In the classic formulation of the model, a nonconserved order parameter $\phi(\mathbf{x},t)$ characterizes the phase of the system at each point. A suitable free energy (or entropy) functional is then constructed, which depends on the order parameter as well as on the associate (conserved) fields and their gradients. The extremization of the functional with respect to these variables results in the dynamic equations for the evolution of the process. Studies conducted on solidification of both pure substances and binary alloys [5–18] pointed out that the model incorporates in a natural fashion the effects of the interface curvature and nonequilibrium phenomena as the trapping of solute into the solid phase and the kinetic undercooling of the solid-liquid interface. Within this approach, complex phenomena as the formation of solute bands in solidification far from equilibrium and the groove instability in cellular growth [19–21] were described and interpreted. Moreover, the interfacial region is spread along a finite thickness, which gives a more natural and consistent picture of the solidification front.

An extension of the phase-field model to incorporate flow effects was first proposed by Caginalp and Jones [22,23]. They derived a system of differential equations for the variables temperature, order parameter, fluid velocity, density, and pressure. In the momentum equation, capillary and viscosity effects were neglected. An asymptotic analysis showed the effects of the advection flow on the interface kinetics.

In a subsequent study, Oxtoby [24] considered density change effects in crystal growth starting from a thermody-

namic potential in which, besides the nonconserved phase field, also the local density ρ is regarded as a (conserved) order parameter. The dynamic equation for the growth rate results from the extremization of the potential with respect to the phase field, and the Navier-Stokes equation is written in the interfacial region using an expression for the capillary stress tensor that is derived resorting to density functional arguments. Then, the coupled problem to determine the growth rate and the flow field is stated through the above equations and the mass conservation condition. Steady state solutions of the model, obtained in isothermal conditions, put in evidence the role of sound modes in density transport.

Anderson *et al.* [25] developed a phase-field model with convection in the melt, deriving an expression for the stress tensor within the arguments of the extended irreversible thermodynamics. The problem was treated in the quasi-incompressibility approximation, neglecting the pressure dependence of the local density, which is assumed uniform in the two bulk phases. The condition of positive entropy production, along with the conservation equations for mass, momentum, and energy, was employed to derive the governing equations of the model. In a subsequent study, the same authors [26] examined the sharp interface limit of the model. Their analysis recovered the standard interfacial conditions, including the Young-Laplace and Clausius-Clapeyron equations for the mechanical and chemical equilibrium at the interface.

Conti [27] followed a different approach, starting from a grand canonical potential which includes the local density as a dynamic variable. Square gradient terms were allowed for both the structural order parameter and the density field. The stress tensor was derived assuming that any dissipation of tensorial order should be ascribed to the fluid viscosity. In this formulation, the pressure field is consistently related to the local density via an equation of state. The model equations for the order parameter and the local density, momentum, and energy allow to describe the solidification process and the flow field, including the propagation of elastic waves. The model was numerically solved in one dimension to assess the effects of the fluid convection on the growth dynamics. In the early stage of the growth, significant deviations were observed with respect to the standard diffusive dynamics; these effects may become important in the interpretation of nucleation and postnucleation processes. At late times, when the pressure waves are reabsorbed, the interface velocity evolves with a power law very close to the diffusive dependence $\sim t^{1/2}$.

The extension of the phase-field model to incorporate hydrodynamic effects has been limited in the past to the solidification of pure substances. As many advanced materials utilize alloys with properties highly sensitive to the growth conditions, a further step should consider the extension of the model to alloy solidification.

In this paper, we present a phase-field model for alloy solidification that incorporates in a thermodynamically consistent way flow effects due to density change. The solid phase is modeled as an isotropic fluid with a viscosity much larger than that of the liquid. The model extends our previous study [27] aimed at solidification of pure substances. We start identifying a suitable grand canonical potential whose natural variables are the order parameter, density, solute concentration, and temperature. The entropy production equation, coupled with the balance of mass, momentum, and energy, is used to derive governing equations that drive the system towards equilibrium. The scalar part of the entropy production fixes the dynamic equation for the structural order parameter. The vector contributions reduce in the bulk phases to the classic Fourier expression for the heat flux and to the Fick's law for the solute diffusion. A third term, of tensorial character, allows to find an expression for the stress tensor, starting from the assumption that this contribution is only due to viscous dissipation. This form of the capillary tensor satisfies the Euler-Lagrange conditions for the grand canonical potential when the system is in equilibrium.

The equations of the model have been solved numerically in one dimension, both in the isothermal limit and simulating a directional solidification experiment. The aim of our simulations was to check whether flow effects significantly alter the interface dynamics and the nonequilibrium solute redistribution across the moving front. This latter phenomenon, termed ''solute trapping,'' reflects on the behavior of the partition coefficient k (the ratio of the solute concentration in the growing solid to that in the liquid at the interface), which deviates from its equilibrium value k_e, approaching unity at large growth rates. We observe that the advection flow does not alter the structure of the solid-liquid interface. Then, the interface solute segregation and the trapping phenomenon are almost unaffected by the flow field. On the contrary, the interface mobility is strongly reduced as the fluid velocity increases. This reflects on the dependence of the interface temperature T_I on the growth rate v_I: the region of the unstable (ascending) branch is reduced, and the maximum of the $T_I(v_I)$ curve is found at lower velocities. As a consequence, for isothermal growth the border between the steady and the diffusive regime is slightly shifted. In directional solidification, the change of the $T_I(v_I)$ curve should affect the onset of the oscillatory instability, which is responsible for the formation of solute bands in the solid.

The paper is organized as follows: in Sec. II, the equilibrium of a two-phase system will be analyzed. The dynamic equations of the model will be derived in Sec. III, using the concepts of the extended irreversible thermodynamics. In Sec. IV, we present the scheme for the numerical solution of the model, and in Sec. V the results of the numerical simulations will be discussed. The conclusions will follow in Sec. VI.

II. EQUILIBRIUM OF A TWO-PHASE SYSTEM

A. Closed systems

Let us consider an ideal solution with components A (solvent) and B (solute). The system is assumed in a two-phase equilibrium, at fixed temperature T and volume V; no mass transfer is allowed through the boundaries of V, with M_A, M_B, and the total mass $M=M_A+M_B$ being held fixed. The local state of the system is characterized by a coarse grained density $\rho(\mathbf{x},t)$, the local mass fraction of solute $c(\mathbf{x},t)$, and a nonconserved order parameter $\phi(\mathbf{x},t)$ which is assumed to

take the values $\phi=0$ in the solid and $\phi=1$ in the liquid. Notice that an equivalent description could be given replacing ρ,c with the partial mass densities $\rho_A=\rho(1-c)$ and $\rho_B=\rho c$ [28].

We postulate a generalized Helmholtz free energy density of the form

$$\psi'(\phi,\rho,c,T,\nabla\phi,\nabla\rho,\nabla c)=\psi(\phi,\rho,c,T)+\frac{1}{2}\epsilon_F^2(\nabla\phi)^2+\frac{1}{2}\delta_F^2(\nabla\rho)^2+\frac{1}{2}\eta_F^2(\nabla c)^2, \tag{1}$$

where $\psi(\phi,\rho,c,T)$ is the bulk free energy density and the gradient terms account for nonlocal contributions in the interfacial region. We assume that $\epsilon_F,\delta_F,\eta_F$ depend only on temperature. We wish to derive the equations for the spatial variation of ϕ,ρ,c. Minimizing the total Helmoltz free energy, with the constraint of constants M_A,M_B gives

$$\delta(F-\mu_{0A}M_A-\mu_{0B}M_B)=\delta\int[\psi'-\mu_{0A}\rho(1-c)-\mu_{0B}\rho c]dv=0, \tag{2}$$

where μ_{0A},μ_{0B} are the Lagrange multipliers for the constrained problem; the corresponding Euler-Lagrange equations read

$$\epsilon_F^2\nabla^2\phi-\frac{\partial w}{\partial\phi}=0,\quad \delta_F^2\nabla^2\rho-\frac{\partial w}{\partial\rho}=0,\quad \eta_F^2\nabla^2 c-\frac{\partial w}{\partial c}=0, \tag{3}$$

where

$$w(\phi,\rho,c,T)=\psi[\phi(\mathbf{r}),\rho(\mathbf{r}),c(\mathbf{r}),T]-\mu_{0A}(T)\rho(\mathbf{r})[1-c(\mathbf{r})]-\mu_{0B}(T)\rho(\mathbf{r})c(\mathbf{r}). \tag{4}$$

Let us consider the planar one-dimensional case, with the solutions depending only on the z coordinate. In the bulk phases, recalling that $\partial\psi/\partial\rho=(1-c)\mu_A+c\mu_B$ and $\partial\psi/\partial c=\rho(\mu_B-\mu_A)$, where μ_A,μ_B represent the chemical potential of A or B, Eqs. (3) and (4) reduce to

$$\mu_{A,s}=\mu_{A,l}=\mu_{0A},\quad \mu_{B,s}=\mu_{B,l}=\mu_{0B},\quad \left(\frac{\partial\psi}{\partial\phi}\right)_{\phi=\phi_s}=\left(\frac{\partial\psi}{\partial\phi}\right)_{\phi=\phi_l}=0, \tag{5}$$

where the subscripts s,l indicate the physical properties in the bulk solid and liquid phases, respectively. Multiplying the three Eqs. (3) by ϕ_z,ρ_z,c_z, respectively, and adding them together, we obtain, through simple integration

$$\frac{1}{2}(\epsilon_F^2\phi_z^2+\delta_F^2\rho_z^2+\eta_F^2c_z^2)-w(\phi,\rho,c,T)=P_0(T). \tag{6}$$

Here $P_0(T)$ is clearly the coexistence pressure at temperature T, since in the bulk, where $\phi_z,\rho_z,c_z=0$ it reduces to the usual expression $p=\rho[(1-c)\mu_A+c\mu_B]-\psi$. Equations (5) and (6) define the chemical and mechanical equilibrium of the two-phase system. Equations (1) and (6) allow to find a simple expression for the surface tension. We rewrite Eq. (6) as

$$(\epsilon_F^2\phi_z^2+\delta_F^2\rho_z^2+\eta_F^2c_z^2)-\psi'[\phi(z),\rho(z),c(z),T]+\rho[(1-c)\mu_A+c\mu_B]=P_0(T). \tag{7}$$

When Eq. (7) is integrated over the total volume of the system (from $-L$ far in the solid to $+L$ far into the liquid), it can be written as

$$F=\mu_{0A}M_A+\mu_{0B}M_B-P_0V+\gamma A, \tag{8}$$

where A is the system cross section and the surface tension γ is given by

$$\gamma=\int_{-L}^{+L}(\epsilon_F^2\phi_z^2+\delta_F^2\rho_z^2+\eta_F^2c_z^2)dz. \tag{9}$$

This result extends to a solid-liquid phase transition with density change well known results obtained either for fluid-fluid interfaces or for solidification without density change.

B. Equilibrium for an open system

When the mass constraint is relaxed, the variational problem must refer to the functional [29]

$$\Omega=\int[w'(\phi,\rho,c,T,\nabla\phi,\nabla\rho,\nabla c)]dv\equiv\int\left[w(\phi,\rho,c,T)+\frac{1}{2}\epsilon_F^2(\nabla\phi)^2\frac{1}{2}\delta_F^2(\nabla\rho)^2+\frac{1}{2}\eta_F^2(\nabla c)^2\right]dv, \tag{10}$$

where $w(\phi,\rho,c,T)$, is given by Eq. (4), and reduces to the grand canonical potential for the bulk phases in equilibrium. The corresponding Euler-Lagrange equations still read [see Eqs. (3)]

$$\frac{\partial w'}{\partial\phi}-\frac{\partial}{\partial x_i}\left(\frac{\partial w'}{\partial\phi_i}\right)=0,\quad \frac{\partial w'}{\partial\rho}-\frac{\partial}{\partial x_i}\left(\frac{\partial w'}{\partial\rho_i}\right)=0,\quad \frac{\partial w'}{\partial c}-\frac{\partial}{\partial x_i}\left(\frac{\partial w'}{\partial c_i}\right)=0, \tag{11}$$

where ϕ_i,ρ_i,c_i indicate spatial derivatives with respect to the coordinate x_i. Here and in the following, the summation convention over repeated indexes is used; an explicit dependence of the function w on its variables will be given later.

C. The capillary stress tensor

The equilibrium conditions (11) allow to find a general expression for the capillary stress tensor. Let us denote $\partial_i\equiv\partial/\partial x_i$, and calculate the gradient of the grand canonical potential density considering T as a constant parameter:

$$\partial_i w' = \left(\frac{\partial w'}{\partial \phi}\right)\phi_i + \left(\frac{\partial w'}{\partial \rho}\right)\rho_i + \left(\frac{\partial w'}{\partial c}\right)c_i + \left(\frac{\partial w'}{\partial \phi_k}\right)\phi_{ki} + \left(\frac{\partial w'}{\partial \rho_k}\right)\rho_{ki} + \left(\frac{\partial w'}{\partial c_k}\right)c_{ki}. \quad (12)$$

Using the Euler-Lagrange equations (11) in Eq. (12) yields

$$\partial_i T_{ik} = 0, \quad (13)$$

where

$$T_{ik} = \delta_{ik} w' - \phi_i\left(\frac{\partial w'}{\partial \phi_k}\right) - \rho_i\left(\frac{\partial w'}{\partial \rho_k}\right) - c_i\left(\frac{\partial w'}{\partial c_k}\right) = \delta_{ik} w' - \epsilon_F^2 \phi_i \phi_k - \delta_F^2 \rho_i \rho_k - \eta_F^2 c_i c_k. \quad (14)$$

Equation (13) states the mechanical equilibrium of the system, in terms of an intrinsically symmetric capillary tensor **T** whose components are defined through Eq. (14) (δ_{ik} is the Kronecker symbol). We show in the following section that **T** represents the nondissipative part of the overall stress tensor. An alternative form of Eq. (14) can be given observing that $w = -p + \rho(\partial w/\partial \rho)$ and using the second of Eqs. (3):

$$T_{ik} = \delta_{ik}\left[-p + \rho\delta_F^2 \nabla^2 \rho + \frac{1}{2}\epsilon_F^2 (\nabla \phi)^2 + \frac{1}{2}\delta_F^2 (\nabla \rho)^2 + \frac{1}{2}\eta_F^2 (\nabla c)^2\right] - \epsilon_F^2 \phi_i \phi_k - \delta_F^2 \rho_i \rho_k - \eta_F^2 c_i c_k, \quad (15)$$

i.e., in the diagonal part of **T** the contribution due to the bulk pressure is clearly decoupled from the interface terms. In the case of a planar interface normal to z, Eq. (14) along with the Euler-Lagrange conditions yields

$$T_{zz} = -P_0, \quad T_{xx} = T_{yy} = -P_0 + \epsilon_F^2 \phi_i \phi_k + \delta_F^2 \rho_i \rho_k + \eta_F^2 c_i c_k, \quad T_{xz} = T_{yz} = T_{xy} = 0, \quad (16)$$

and the surface tension is given by

$$\gamma = \int_{-L}^{+L} (T_{xx} - T_{zz}) dz. \quad (17)$$

Thus we see that the difference between the stress normal to the interface and the tangential stress is the surface tension per unit length. This result is well known from the analysis of the equilibrium of fluid-fluid interfaces (see, for example, Ref. [30]), and has been recovered here in a more general context. To summarize, for a planar interface the equilibrium profile for the phase, density, and concentration fields is governed by

$$\partial_z T_{zz} = 0, \quad \epsilon_F^2 \phi_{zz} - \left(\frac{\partial w}{\partial \phi}\right) = 0, \quad \eta_F^2 c_{zz} - \left(\frac{\partial w}{\partial c}\right) = 0, \quad \frac{\partial \rho}{\partial t} = 0, \quad (18)$$

along with the condition of uniform and constant temperature. In the following section, we shall derive the dynamic equations for an out of equilibrium system.

III. THE DYNAMIC EQUATIONS

A. The entropy production rate

We now address the nonequilibrium situation through a thermodynamic procedure, starting from the local balance of mass, momentum, energy, and entropy. Let us denote the velocity field by **v**, the specific energy by e', and the specific entropy by s'. The two latter quantities are determined by the specific free energy $f'(\phi, \rho, c, T, \nabla\phi, \nabla\rho, \nabla c,)$ and in general involve gradient contributions. The stress tensor will be denoted by **P**; $\mathbf{J}_E$, $\mathbf{J}_S$, $\mathbf{J}_D$ stand for the energy, entropy, and solute flux vectors, respectively, and σ is the entropy production rate. Finally, **g** stands for a specific body force field. In terms of these variables the classical balance laws read

$$\frac{d\rho}{dt} = -\rho \nabla \cdot \mathbf{v}, \quad (19)$$

$$\rho \frac{dc}{dt} = -\nabla \cdot \mathbf{J}_D, \quad (20)$$

$$\rho \frac{d\mathbf{v}}{dt} = \rho \mathbf{g} - \nabla \cdot \mathbf{P}, \quad (21)$$

$$\rho \frac{de'}{dt} = -\nabla \cdot \mathbf{J}_E - \mathbf{P} : \nabla \mathbf{v}, \quad (22)$$

$$\rho \frac{ds'}{dt} = -\nabla \cdot \mathbf{J}_S + \sigma. \quad (23)$$

The constitutive relations and the explicit form of the fluxes will follow from the Courie principle and from the local form of the second law of thermodynamics, which implies $\sigma \geqslant 0$. In addressing the solid-liquid transition we will assume that the solid phase is at rest.

The specific Helmoltz free energy is given by

$$f'(\phi, \rho, c, T, \nabla\phi, \nabla\rho, \nabla c) = \frac{1}{\rho}\psi'(\phi, \rho, c, T, \nabla\phi, \nabla\rho, \nabla c) = f(\phi, \rho, c, T) + \frac{1}{2\rho}[\epsilon_F^2 (\nabla\phi)^2 + \delta_F^2 (\nabla\rho)^2 + \eta_F^2 (\nabla c)^2], \quad (24)$$

where $f(\phi, \rho, c, T) = \psi(\phi, \rho, c, T)/\rho$ is the specific bulk free energy. The nongradient parts of the specific energy and entropy are defined by

$$s(\phi, \rho, c, e) = -\frac{\partial f}{\partial T}, \quad e(\phi, \rho, c, s) = f(\phi, \rho, c, T) + Ts(\phi, \rho, c, e). \quad (25)$$

Similar relations are postulated for the corresponding quantities incorporating gradient terms. Denoting

$$\epsilon_S^2 \equiv \frac{d\epsilon_F^2}{dT}, \quad \delta_S^2 \equiv \frac{d\delta_F^2}{dT}, \quad \eta_S^2 \equiv \frac{d\eta_F^2}{dT}, \tag{26}$$

$$\epsilon_E^2 = \epsilon_F^2 - T\epsilon_S^2, \quad \delta_E^2 = \delta_F^2 - T\delta_S^2, \quad \eta_E^2 = \eta_F^2 - T\eta_S^2,$$

we obtain from Eq. (24)

$$s'(\phi,\rho,c,e,\nabla\phi,\nabla\rho,\nabla c) = s(\phi,\rho,c,e) - \frac{1}{2\rho}[\epsilon_S^2(\nabla\phi)^2 + \delta_S^2(\nabla\rho)^2 + \eta_S^2(\nabla c)^2], \tag{27}$$

$$e'(\phi,\rho,c,s,\nabla\phi,\nabla\rho,\nabla c) = e(\phi,\rho,c,s) + \frac{1}{2\rho}[\epsilon_E^2(\nabla\phi)^2 + \delta_E^2(\nabla\rho)^2 + \eta_E^2(\nabla c)^2]. \tag{28}$$

Under the above assumptions the differential form of the second law of thermodynamics reads

$$\begin{aligned} T\,ds' = de' &- \frac{\partial f}{\partial\phi}d\phi - \frac{1}{\rho^2}\left[p - \frac{1}{2}\epsilon_F^2(\nabla\phi)^2 - \frac{1}{2}\delta_F^2(\nabla\rho)^2 - \frac{1}{2}\eta_F^2(\nabla c)^2\right]d\rho - (\mu_B - \mu_A)dc \\ &- \frac{1}{\rho}[\epsilon_F^2(\nabla\phi)d(\nabla\phi) + \delta_F^2(\nabla\rho)d(\nabla\rho) + \eta_F^2(\nabla c)d(\nabla c)]. \end{aligned} \tag{29}$$

Combining Eq. (29) with the balance equations (19), (21), and (23) yields, after some manipulations

$$\begin{aligned} \rho\frac{ds'}{dt} = &-\frac{\nabla\cdot\mathbf{J}_E}{T} - \frac{\epsilon_F^2}{T}\nabla\cdot\left(\frac{d\phi}{dt}\nabla\phi\right) - \frac{\delta_F^2}{T}\nabla\cdot\left(\frac{d\rho}{dt}\nabla\rho\right) \\ &- \frac{\eta_F^2}{T}\nabla\cdot\left(\frac{dc}{dt}\nabla c\right) - \frac{1}{T}\frac{d\phi}{dt}\left(\rho\frac{\partial f}{\partial\phi} - \epsilon_F^2\nabla^2\phi\right) \\ &- \frac{1}{T}(P_{ik} + T_{ik})\partial_i v_k + \frac{(\mu_B - \mu_A)}{T}\nabla\cdot\mathbf{J}_D \\ &+ \frac{\eta_F^2\nabla^2 c}{T}\frac{dc}{dt}, \end{aligned} \tag{30}$$

where T_{ik} is the capillary stress tensor defined by Eq. (15) and rewritten, out of equilibrium, as

$$T_{ik} = \delta_{ik}\left(w' - \rho\frac{\delta\Omega}{\delta\rho}\right) - \epsilon_F^2\phi_i\phi_k - \delta_F^2\rho_i\rho_k - \eta_F^2 c_i c_k. \tag{31}$$

We can rearrange Eq. (30) according to the entropy balance equation (23) adopting an entropy flux

$$\mathbf{J}_S = \frac{1}{T}\left\{\mathbf{J}_E + \epsilon_F^2\frac{d\phi}{dt}\nabla\phi + \delta_F^2\frac{d\rho}{dt}\nabla\rho + \eta_F^2\frac{dc}{dt}\nabla c + \left[(\mu_B - \mu_A) + \frac{(\eta_F^2\nabla^2 c)}{\rho}\right]\mathbf{J}_D\right\}. \tag{32}$$

Finally we find

$$\rho\frac{ds'}{dt} = -\nabla\cdot\mathbf{J}_S + \sigma, \tag{33}$$

where the entropy production rate σ is given by

$$\begin{aligned} \sigma = &-\frac{1}{T}\frac{d\phi}{dt}\left(\rho\frac{\partial f}{\partial\phi} - \epsilon_F^2\nabla^2\phi\right) + \mathbf{J}_E\cdot\nabla\left(\frac{1}{T}\right) \\ &+ \frac{d\phi}{dt}\nabla\phi\cdot\nabla\left(\frac{\epsilon_F^2}{T}\right) + \frac{d\rho}{dt}\nabla\rho\cdot\nabla\left(\frac{\delta_F^2}{T}\right) + \frac{dc}{dt}\nabla c\cdot\nabla\left(\frac{\eta_F^2}{T}\right) \\ &+ \mathbf{J}_D\cdot\nabla\left[\frac{(\mu_A - \mu_B)}{T} + \eta_F^2\frac{\nabla^2 c}{\rho T}\right] - \frac{1}{T}(\mathbf{P} + \mathbf{T}):\nabla\mathbf{v}. \end{aligned} \tag{34}$$

As observed by Charach and Fife [31], the nonclassical contributions of the above equation (third, fourth, and fifth terms in the right-hand side) can be treated, according to the Courier's principle, as either of vectorial or of scalar origin, depending on the way in which the corresponding thermodynamic forces or fluxes are defined. However, to simplify the discussion, extending the choice of Wang *et al.* in their model for solidification at constant density [9], we assume that $\epsilon_E^2 = \delta_E^2 = \eta_E^2 = 0$, so that $e = e'$, and $\epsilon_S^2, \delta_S^2, \eta_S^2 = \text{const}$. Moreover, in the sequel we shall neglect the spatial variation of ϵ_F^2, δ_F^2, and η_F^2, which amounts to neglect the thermal gradient across the interface. Then, the constraint of local positive entropy production reduces to

$$\frac{d\phi}{dt} = -\Gamma\left(\rho\frac{\partial f}{\partial\phi} - \epsilon_F^2\nabla^2\phi\right), \tag{35}$$

$$\mathbf{J}_E = -K\nabla T, \tag{36}$$

$$\mathbf{J}_D = M_c\nabla\left[\frac{(\mu_A - \mu_B)}{T} + \eta_F^2\frac{\nabla^2 c}{\rho T}\right], \tag{37}$$

where M_c, Γ are positive constants and K is the thermal conductivity. Moreover, assuming that the tensor contribution is only amenable to viscous dissipation, we obtain

$$\mathbf{P} = -\mathbf{T} - \mathbf{\Pi}, \tag{38}$$

with $\mathbf{\Pi}$ indicating the standard stress tensor for viscous fluids. We anticipate here that in the following we shall consider the solid phase as an isotropic fluid with a viscosity much larger than that of the liquid phase.

B. The thermodynamic potential

To proceed further we need an explicit form for the specific free energy f. At first, we construct a suitable expression for a pure substance. In this case the potential should take the

form of a double well over the ρ,ϕ plane, with the two minima centered at the bulk solid ($\rho=\rho_{s0},\phi=0$) and liquid ($\rho=\rho_{l0},\phi=1$), where we denoted as ρ_{s0}, ρ_{l0} the equilibrium densities in the two phases at some reference temperature T_0 and pressure p_0. We start from a linearized equation of state of the type

$$\rho-\rho_0=-\beta\rho_0(T-T_0)+k\rho_0(p+\mathcal{P}-p_0), \tag{39}$$

where β is the thermal expansion coefficient and k is the isothermal compressibility; p is the thermodynamic pressure given by $p=\rho^2(\partial f/\partial\rho)$ and $\mathcal{P}$ is the excess pressure due to the capillary stress. In the case of a planar interface normal to z, the latter is written as $\mathcal{P}=(\epsilon_F^2\phi_z^2+\delta_F^2\rho_z^2+\eta_F^2c_z^2)/2-\rho\delta_F^2\rho_{zz}$.

An expression of the free energy, consistent with Eq. (39) may be written as

$$\begin{aligned}f(\rho,\phi,T)=&\frac{ag(\phi)}{\rho}+\frac{\beta}{k}(T-T_0)\left[\frac{\rho-\rho_0(\phi)}{\rho\rho_0(\phi)}\right]+(p_0-\mathcal{P})\\&\times\left[\frac{\rho-\rho_0(\phi)}{\rho\rho_0(\phi)}\right]-CT\ln\frac{T}{T_0}+C(T-T_0)\\&+p(\phi)L_0\left(1-\frac{T}{T_0}\right)-\frac{(p_0-\mathcal{P})}{\rho_0(\phi)}\\&+\frac{\rho_0(\phi)}{2k}\left[\frac{\rho-\rho_0(\phi)}{\rho\rho_0(\phi)}\right]^2,\end{aligned} \tag{40}$$

with $g(\phi)=(1/4)\phi^2(1-\phi)^2$. In Eq. (40), C is the specific heat and L_0 is the latent heat per unit mass in the reference state. We observe a Landau-Ginzburg contribution for the order parameter ϕ (first term in the right-hand side of the equation), and the elastic contribution of the last term. Along the way followed by Ref. [23] we shall neglect in the pressure field the contribution due to the density dependence of the well height. The function $p(\phi)$ is monotonic and increasing with ϕ, assuming the values $p(0)=0$, $p(1)=1$, and describes the transition of the free energy from the solid to the liquid phase. Choosing $p(\phi)=\phi^3(10-15\phi+6\phi^2)$ fixes the bulk solid and liquid to the values $\phi=0$ and $\phi=1$, respectively, for every value of temperature. The equilibrium density $\rho_0(\phi)$ is assumed to change in the interfacial region as $\rho_0\equiv\rho_0(\phi)=\rho_{s0}+p(\phi)(\rho_{l0}-\rho_{s0})$.

For an ideal binary alloy, the specific free energy is written as

$$f=(1-c)\left[f_A+\frac{RT}{\overline{M}}\ln(1-c)\right]+c\left[f_B+\frac{RT}{\overline{M}}\ln c\right], \tag{41}$$

where R is the gas constant, and f_A,f_B represent the free energy of the pure components A and B obtained by replacing in Eq. (40) the material parameters with the ones of the solvent and the solute, respectively, and the equilibrium density with

$$\rho_0(\phi)=\frac{\rho_{0A}\rho_{0B}}{(1-c)\rho_{0B}+c\rho_{0A}}. \tag{42}$$

To simplify the discussion, here and in the sequel we neglect the difference of the molar mass $\overline{M}$ of the two components, assuming $\overline{M}_A=\overline{M}_B\equiv\overline{M}$, that means to identify the molar concentration with the mass fraction.

Then, the solute flux $\mathbf{J}_D$ may be expressed as

$$\begin{aligned}\mathbf{J}_D=&-\frac{M_cR}{\overline{M}c(1-c)}\nabla c+M_c\nabla\left(\frac{\eta_F^2}{\rho T}\nabla^2c\right)\\&+M_c\nabla\left\{\frac{(a_A-a_B)}{\rho T}g(\phi)+\frac{p(\phi)}{T}\left[L_{0A}\left(1-\frac{T}{T_{0A}}\right)\right.\right.\\&\left.\left.-L_{0B}\left(1-\frac{T}{T_{0B}}\right)\right]\right\}.\end{aligned} \tag{43}$$

We recover the standard definition of the solute diffusivity D_c taking

$$D_c=\frac{M_cR}{\rho\overline{M}c(1-c)}. \tag{44}$$

As the solute diffusivity is quite different in the solid and liquid phases, in the following D_c will be taken as $D_c=D_s+p(\phi)(D_l-D_s)$, D_l and D_s being the diffusivities in the liquid and in the solid, respectively. In the same spirit we represent the local viscosity as $\eta=\eta_s+p(\phi)(\eta_l-\eta_s)$, with $\eta_s\gg\eta_l$.

To complete the model we assume that, along a solid-liquid transition, the internal energy changes as

$$\begin{aligned}e\equiv(1-c)e_A+ce_B=&(1-c)e_{sB}+ce_{sB}+p(\phi)[(1-c)L_{0A}\\&+cL_{0B}].\end{aligned} \tag{45}$$

Then, Eqs. (19)–(22) and (35), along with specifications (36), (38), (43), and (45), represent the evolution equations for the system.

C. Nondimensional equations in one dimension

The governing equations can be written in nondimensional form adopting a reference length ξ and scaling time to $\tau=\xi^2/D_l$. Density is scaled to ρ_{l0A} and a nondimensional temperature is introduced as $u=C_p(T-T_{0A})/L_{0A}$, where C_p is the the specific heat at constant pressure. Pressure and the components of the stress tensor are scaled to $\rho_{l0A}v_0^2$, where $v_0=\xi/\tau$ is the natural reference for velocities. Notice that in the following we neglect thermal expansion effects and we assume equal compressibilities in both phases. Retaining for simplicity the same symbols for the scaled (nondimensional) quantities, and in absence of body forces, the model equations in one dimension read

$$\frac{\partial\rho}{\partial t}+v\frac{\partial\rho}{\partial z}=-\rho\frac{\partial v}{\partial z}, \tag{46}$$

$$\frac{\partial \phi}{\partial t}+v\frac{\partial \phi}{\partial z}=m\frac{\partial^2 \phi}{\partial z^2}-\frac{m}{\tilde{\epsilon}^2}g'(\phi)[(1-c)+c\omega_1]$$
$$-\rho p'(\phi)\beta_1\left[(1-c)\left(1-\frac{T}{T_{0A}}\right)+c\omega_2\left(1-\frac{T}{T_{0B}}\right)\right]-\frac{1}{2}\beta_2\rho p'(\phi)[(1-c)(1-S_A)+c(E-S_B)]\left(\frac{\rho_0^2-\rho^2}{\rho^2\rho_0^2}\right), \quad (47)$$

$$\rho\frac{\partial v}{\partial t}+\rho v\frac{\partial v}{\partial z}=-\nabla\cdot\left[\beta_3\frac{(\rho-\rho_0)}{\rho}\right]+\beta_4\frac{\partial}{\partial z}\left(\lambda_1(\phi)\frac{\partial v}{\partial z}\right), \quad (48)$$

$$\rho\frac{\partial c}{\partial t}+\rho v\frac{\partial c}{\partial z}=-\frac{\partial}{\partial z}\lambda_2(\phi)\rho c(1-c)\frac{\partial}{\partial z}\left\{\ln\frac{1-c}{c}+\frac{T_{0A}}{T}\beta_5 g(\phi)(1-\omega_1)+\frac{T_{0A}}{T}p(\phi)\times\left(\beta_1\beta_5\frac{\tilde{\epsilon}^2}{m}\right)\left[\left(1-\frac{T}{T_{0A}}\right)-\omega_2\left(1-\frac{T}{T_{0B}}\right)\right]+\frac{T_{0A}}{T}\frac{\beta_6}{\rho}\frac{\partial^2 c}{\partial z^2}\right\}, \quad (49)$$

$$\frac{\partial u}{\partial t}+v\frac{\partial u}{\partial z}=-p'(\phi)[(1-c)+c\omega_2]\left(\frac{\partial \phi}{\partial t}+v\frac{\partial \phi}{\partial z}\right)+\frac{D_T}{D_l}\frac{\partial^2 u}{\partial z^2}+\frac{\beta_2\beta_4}{\rho\beta_1\beta_3}\left(\frac{\partial v}{\partial z}\right)^2, \quad (50)$$

where D_T is the thermal diffusivity, and the functions $\lambda_1(\phi)$ and $\lambda_2(\phi)$ are defined as $\lambda_1(\phi)=1+[1-p(\phi)][(\eta_s/\eta_l)-1]$ and $\lambda_2(\phi)=(D_s/D_l)+p(\phi)[1-(D_s/D_l)]$.

The model parameters are defined as

$$m=\frac{\Gamma\epsilon_F^2\tau}{\xi^2},\quad \tilde{\epsilon}^2=\frac{\epsilon_F^2}{a_A\xi^2},\quad \beta_1=\Gamma\tau\rho_{l0A}L_{0A},\quad \beta_2=\frac{\Gamma\tau}{k},$$
$$\beta_3=\frac{1}{k\rho_{l0A}v_0^2}, \quad (51)$$
$$\beta_4=\frac{\eta_l}{\tau\rho_{l0A}v_0^2},\quad \beta_5=\frac{a_A\bar{M}}{\rho_{l0A}RT_{0A}},\quad \beta_6=\frac{\eta_F^2\bar{M}}{\rho_{l0A}\xi^2RT_{0A}},$$
$$\beta_7=\frac{\delta_F^2\rho_{l0A}}{\xi^2v_0^2},$$
$$\omega_1=\frac{a_B}{a_A},\quad \omega_2=\frac{L_{0B}}{L_{0A}},\quad S_A=\frac{\rho_{s0A}}{\rho_{l0A}},\quad S_B=\frac{\rho_{s0B}}{\rho_{l0A}},$$
$$E=\frac{\rho_{l0B}}{\rho_{l0A}}.$$

TABLE I. Values of the model parameters.

Parameter	Value
S_A	1.051
S_B	1.026
E	0.983
ω_1	5.727×10^{-1}
ω_2	6.910×10^{-1}
m	466
$\tilde{\epsilon}$	8×10^{-4}
β_1	8.484×10^{8}
β_2	6.681×10^{10}
β_3	9.231×10^{13}
β_4	1.282×10^{3}
β_5	1.071
β_6	6.853×10^{-7}
β_7	6.440×10^{5}

Notice that imposing $S_A=S_B=E=1$, the density effects are ruled out; if, in addition, we pose $c=0$ or $c=1$ we recover the classic phase-field description for the solidification of a pure substance (A or B, respectively). In this case the model parameters $\epsilon_F, a_{A,B}, \Gamma$ can be related to the material properties through [32]

$$\epsilon_F^2=6\sqrt{2}\sigma_A h_A=6\sqrt{2}\sigma_B h_B,\quad a_A=6\sqrt{2}\frac{\sigma_A}{h_A}, \quad (52)$$
$$a_B=6\sqrt{2}\frac{\sigma_B}{h_B},\quad \Gamma=\frac{\mu_A\sigma_A T_{0A}}{\rho_A L_A\epsilon_F^2}=\frac{\mu_B\sigma_B T_{0B}}{\rho_B L_B\epsilon_F^2},$$

where h is the interface width, σ is the surface tension, and μ is the kinetic undercooling coefficient that relates the interface undercooling to the interface velocity v through $v=\mu(T_0-T)$. We assume that the above equations still represent a good estimation of the model parameters in terms of the thermophysical properties of the material. As we did not allow Γ, ϵ_F to depend on concentration, we force the two conditions $\sigma_A h_A=\sigma_B h_B$ and $\mu_A T_{0A}/(h_A\rho_A L_A)=\mu_B T_{0B}/(h_B\rho_B L_B)$. In case that $h_A\sim h_B$, the latter is amenable to the reasonable assumption that the interface velocity should result proportional to the free energy jump across the interface; indeed, for a nickel-copper alloy the condition is verified within 1%. To estimate δ_F, η_F we assume equal contributions of the gradient terms to the surface tension, i.e., $\rho_l^2\delta_F^2=\epsilon_F^2=\eta_F^2$. To conduct the numerical simulations we referred to the phase diagram of a nickel (solvent) and copper (solute) binary alloy. The interface thickness has been chosen as $h_A=16\times10^{-8}$ cm, and the length scale is $\xi=2\times10^{-4}$ cm. The resulting values of the nondimensional model parameters are summarized in Table I.

IV. THE NUMERICAL METHOD

We conducted two sets of numerical experiments. At first we solved the one-dimensional equations (46)–(49) at fixed and uniform temperature. Then, we simulated a directional

solidification process in which the phase transition is driven by a temperature field moving at constant speed V_P, and characterized by a uniform gradient $G>0$ [in this case, Eq. (50) is modified as $\partial u/\partial t=-V_P G$]. In both cases, the underlying assumption is that heat diffusion is much faster than solute diffusion, so that the temperature field can be decoupled from the concentration and the phase fields.

The equations have been solved on the computational domain $0\leqslant z\leqslant z_m$. Initially, a phase boundary at $z=z_0$ separates a solid region ($z<z_0, \phi=0$) from the liquid region ($z>z_0, \phi=1$). The density in the two phases is selected at the minimum of the potential, and the system is initially at rest, i.e., $v(z,0)=0$. In the first set of simulations (fixed temperature), the concentration is initially uniform below the liquidus line. For directional solidification, the initial concentration in the two phases is fixed at the equilibrium values corresponding to the initial interface temperature. For the phase, density, and concentration fields we imposed Neumann boundary conditions; the velocity is fixed as $v(0,t)=0$ at the left end of the solid, while we chose $(\partial v/\partial z)=0$ at $z=z_m$. To advance the solution forward in time, we employed an explicit Euler integration scheme for the density, concentration, and phase-field equations. To allow the condition $\eta_s \gg \eta_l$, which results in a large diffusion term in the momentum equation, the latter was integrated with a Crank-Nicolson implicit scheme. Second-order central differences were used to discretize the Laplace operator, and upwind differences for the convective terms. To ensure an accurate resolution of the solid-liquid interface, the grid spacing was selected as $\Delta z=0.25\tilde{\epsilon}$; the time step required for numerical stability is $\Delta t=0.12\times 10^{-10}$. Following a standard method in computational fluid dynamics, the velocity field was solved on a computational grid shifted of $\Delta z/2$ with respect to the one used for the scalar fields.

V. THE NUMERICAL RESULTS

A. Isothermal growth

We first checked whether the model gives a consistent description of the mechanical effects due to the density change in solidification. To this aim we solved the model equations at constant temperature, fixing our attention to the mechanical relaxation of the system. The far-field concentration is $c_0=0.072\,14$, and the temperature is selected as $T=1700$ K. This value is well below the T_0 line (the locus where the Helmoltz free energies of the liquid and the solid are equal: at $c=c_0$ we have $T_0=1704.32$ K), ensuring a steady growth regime. The contraction of the liquid in front of the interface originates a pressure wave that propagates both into the solid and into the liquid. This effect is illustrated in Fig. 1, where only the liquid portion of the system is shown. The solid-liquid interface is located near $z=0.64$ (here and in the following, except for temperature, all the numerical results will be presented in nondimensional form), and the pressure field is represented at different times. The initial pressure was initialized as $p(z,0)=0$, and we see the negative pressure front that propagates into the liquid. The velocity of the wave, estimated tracking the position of the wave front, results $v_s=9.60\times 10^6$; this value is in excellent agreement with the theoretical one for the liquid in equilibrium, assumed as a pure elastic medium: the latter is $\sqrt{\partial p/\partial \rho}=\sqrt{\rho_{l0A}\beta_3/\rho_{l0}}=9.61\times 10^6$.

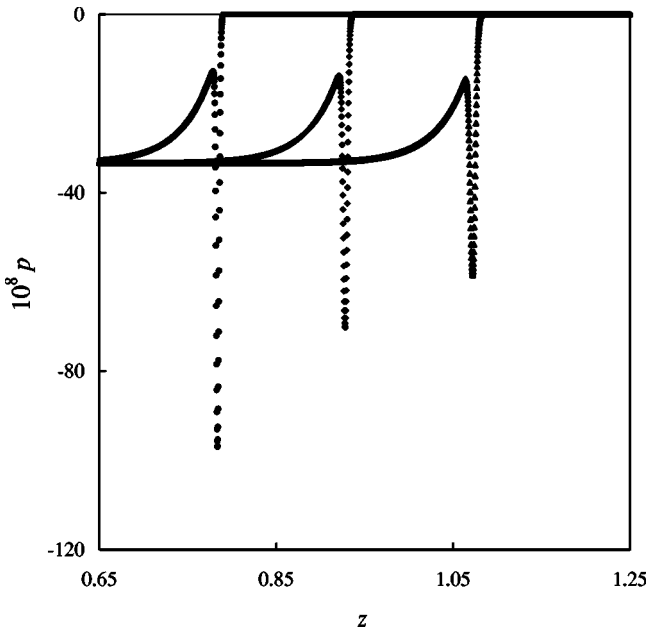

FIG. 1. The pressure wave originated at the solid-liquid interface. The interface is located near $z=0.64$, and the different curves represent the pressure field at times 1.5×10^{-8}, 3.0×10^{-8}, and 4.5×10^{-8} from left to right. The wave speed is $v_s=9.60\times 10^6$. The model parameters are specified in Table I.

After a short transient, these growth conditions result in a steady advancement of the solid-liquid interface. In Figs. 2(a)–2(d), we show the phase, density, velocity, and concentration profiles obtained at different times. We observe that the solid is at rest, while the liquid is advected towards the interface with a velocity $v=-601.81$. The interface velocity, as resulting from the numerical data, is $v_I=11\,927$. Notice that this is the same value fixed by the mass conservation law through the relation $v=(1-\rho_{s0}/\rho_{l0})v_I$. The solid concentration is $c_s=c_0$, while on the liquid side of the interface the concentration peak is $c_l=0.072\,67$. We see that the trapping of solute results in a dynamic partition coefficient $k=c_s/c_l=0.993$, far from equilibrium value $k_e=0.795$.

At higher temperatures, as the T_0 line is approached from below, we observed the expected transition from the kinetic to the diffusive regime. We want now to draw the attention on an interesting point. The flow effects result in a slower interface dynamics (see, for example Ref. [33]). Then, we may expect that in the dynamic phase diagram (in the T,c plane) steady state solutions, due to density change, could be pushed into the region of diffusive regimes. This effect is illustrated in Fig. 3, where the growth rate is represented versus time, at $T=1703$ K. The upper set of data shows the kinetic (steady) growth obtained without density change (i.e., fixing $S_A=S_B=E=1$). In the lower curve we accounted for the density effects, fixing $S_A=S_B=0.8$, $E=1$; in this case the late stage growth is characterized by the diffusive law $v_I\sim t^{-1/2}$.

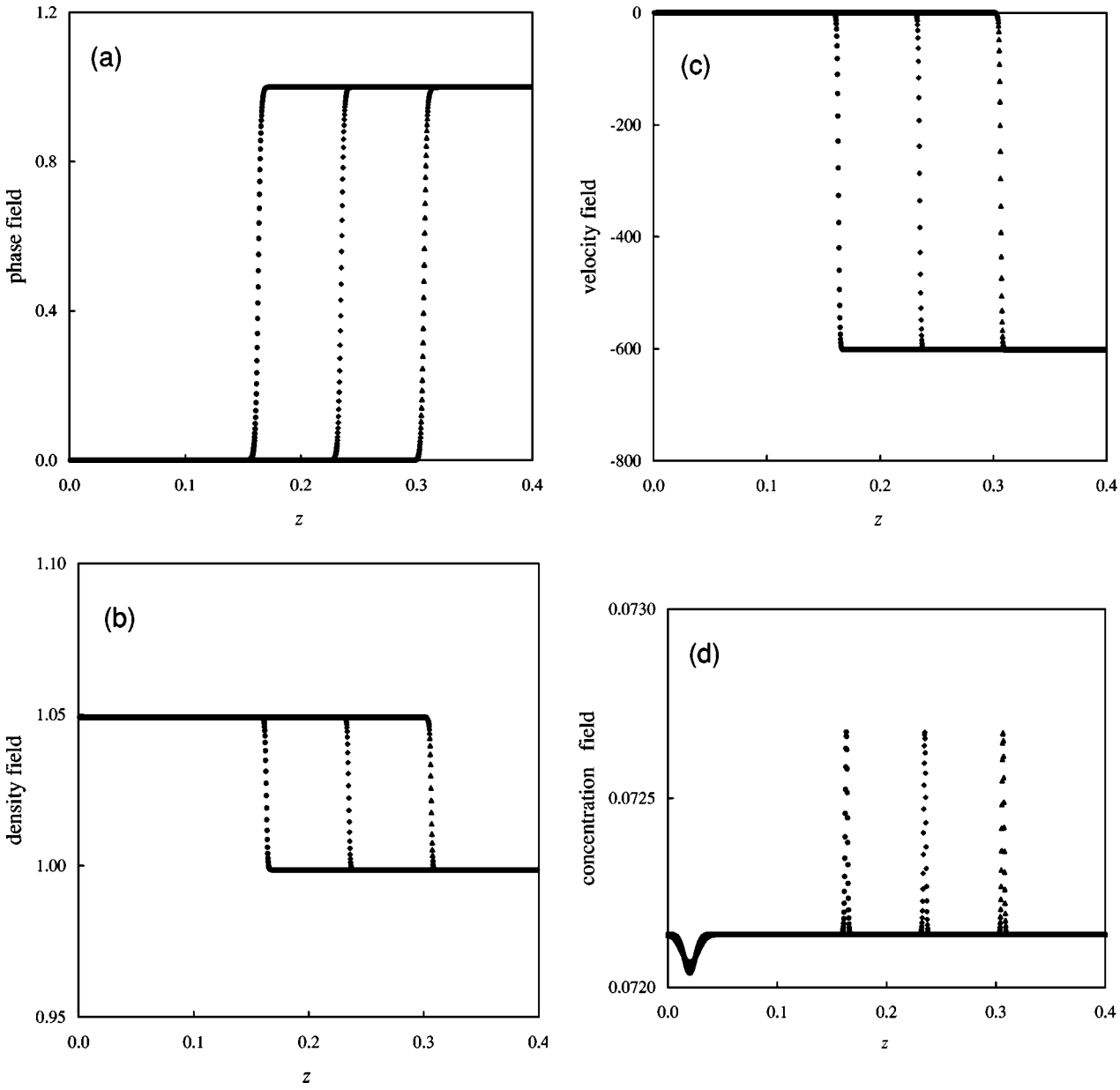

FIG. 2. The phase (a), density (b), velocity (c), and concentration (d) fields at different times. The curves are taken at $t=1.2\times10^{-5}$,$t=1.8\times10^{-5}$,2.4×10^{-5} from left to right. The model parameters are specified in Table I.

B. Directional solidification

The aim of this set of simulations is to determine how and to what extent the volume difference of the two phases affects the trapping of solute and the temperature of the solid-liquid interface.

The initial concentration of the alloy is set to $c_{s0}=0.056\,097$ for the solid phase ($z<z_0$) and $c_{l0}=0.070\,686$ for the liquid phase ($z>z_0$). This corresponds to an equilibrium temperature $T_I=1705.71$ K. Then the initial temperature profile, defined as

$$T(z,0)=T_I+G(z-z_0) \tag{53}$$

is pulled towards the positive z direction with constant velocity V_P. After a transient, the solidification front selects a steady interface temperature T_I, following the advancing isotherms with their same velocity, and the solid phase grows with uniform concentration c_{l0}. The solute segregation on the moving front is evaluated computing the peak of $c(z,t)$, which identifies the concentration c_l on the liquid side of the interface.

We recall that the segregation of solute is interpreted as a diffusive process across the interface, characterized by a velocity scale $v_d=D/a$, where D is the solute diffusivity and a is the interface width. The dependence of the partition coefficient on the growth velocity takes the form [34,35]

$$k(v_I)=\frac{k_e+v_I/v_d}{1+v_I/v_d}. \tag{54}$$

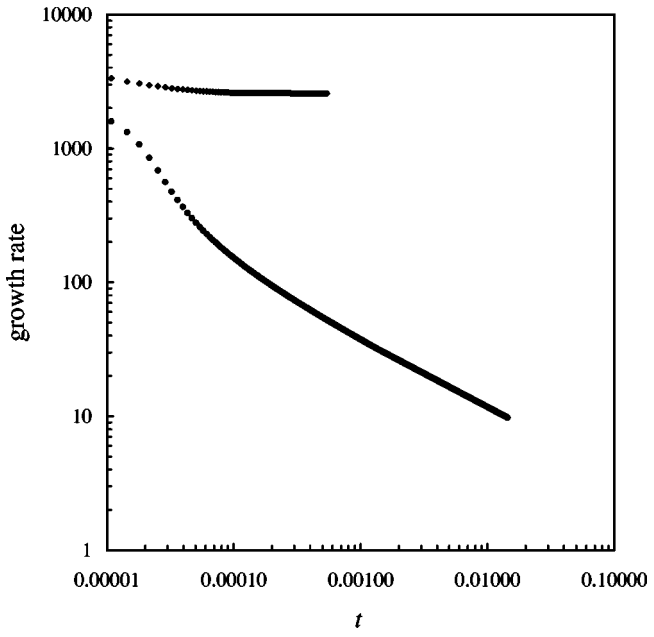

FIG. 3. The growth rate for $T=1703$ K. The upper curve ($S_A=S_B=E=1$) shows the steady regime when density effects are neglected. The flow field shifts the growth regime into the diffusive region (lower curve, $S_A=S_B=0.8$, $E=1$).

In this perspective, the solute segregation could only be affected by a change of the solute transition layer. Figures 4(a) and 4(b) show the concentration field obtained in steady conditions with and without density change, respectively. In both cases we have $G=200$ K and $V_P=800$. Notice that the solute profile is almost unaffected by the flow field. Then, we do not expect significant effects of the density change on the $k(v_I)$ dependence. This prediction is confirmed in Fig. 5, which shows the (normalized) partition coefficient $(k-k_e)/(1-k_e)$ versus the growth rate; the different curves are taken with $E=1$ and $S_A=S_B$ ranging from 1 to 1.2. We observe that the curves are very close to each other, and the k values do not differ for more than 5%.

The dependence of the interface temperature on the interface velocity exhibits a nonmonotonic behavior: due to suppression of solute partitioning (and to the reduction of solute concentration on the liquid side of the interface), at low velocities $T_I(v_I)$ first rises, then falls with increasing v_I reflecting the increasing undercooling required to advance the solidification front. In the previous analysis, we observed that the density effects have almost no influence on the trapping of solute, while they induce a significant dissipation in the interface dynamics. As a result, the descending branch of the $T_I(v_I)$ curve should be pushed towards lower temperatures, and the maximum of the curve should migrate towards lower velocities. This effect is shown in Fig. 6, where the interface temperature is shown versus the interface velocity; the curves are taken with the same values of E,S_A,S_B used in Fig. 5. Notice the strong undercooling which characterizes the high velocity branch of the curves, as the change of volume increases. We should also observe that this behavior extends its effects into other fields of the solidification phenomenology: for example, the onset of the oscillatory instability, which is responsible for the band formation at large growth rates, should be shifted by the density effects towards lower velocities.

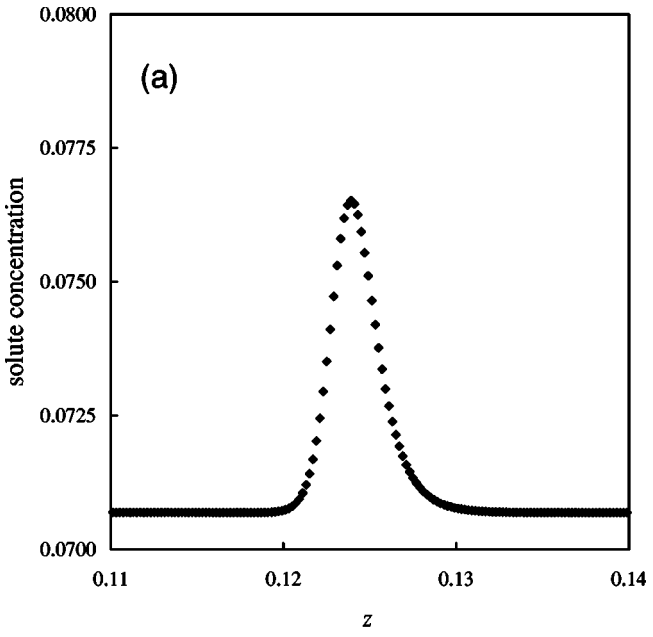

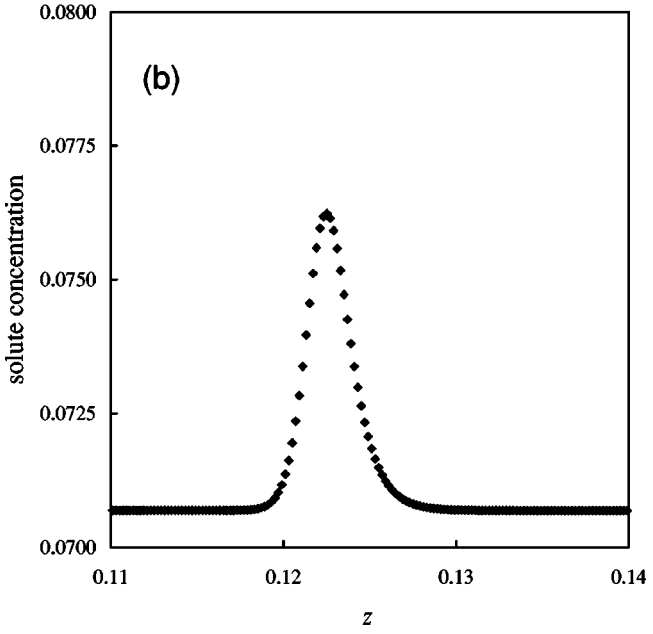

FIG. 4. The solute field in directional solidification with $G=200$ K and $V_P=800$. The upper curve (a) is obtained with $S_A=S_B=E=1$, the lower curve (b) with $S_A=S_B=1.15$, $E=1$. The model parameters are specified in Table I.

VI. CONCLUSIONS

The classical phase-field model is a well established tool to describe solidification far from equilibrium, of both pure substances and binary solutions. However, this method has been exploited assuming equal densities of the solid and liquid phases. In the model presented in this paper, for the

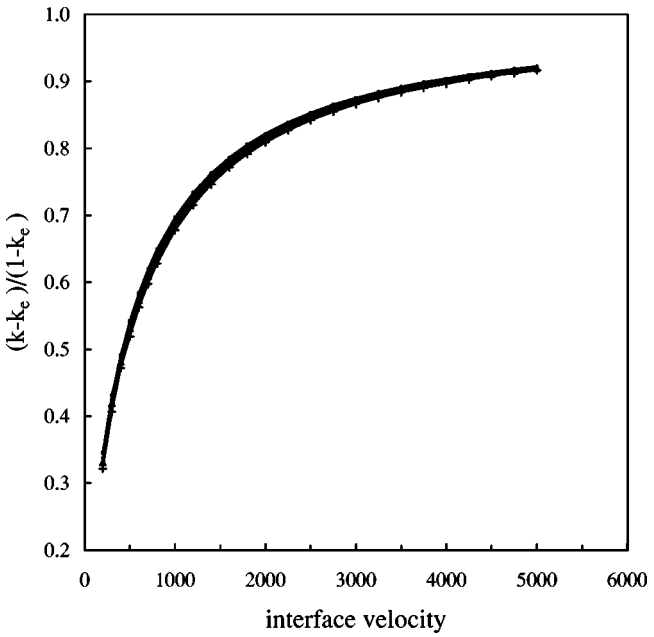

FIG. 5. The (normalized) partition coefficient $(k-ke)/(1-k_e)$ vs the growth rate; the different curves are taken with $E=1$ and $S_A=S_B=1.00,1.05,1.10,1.15,1.20$.

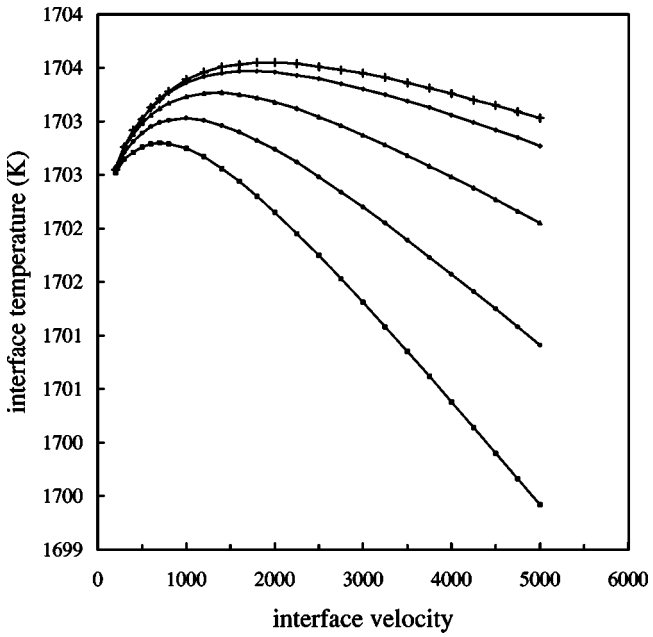

FIG. 6. The interface temperature vs the interface velocity. The curves are obtained with $E=1$ and $S_A=S_B$; from top to down we have $S_A=S_B=1.00,1.05,1.10,1.15,1.20$.

solidification of a binary alloy, this limitation is removed, allowing one to describe the propagation of density waves and the advected flow field. The equations of the model have been derived imposing local positive entropy production, and reduce to the classical formulation for equal solid and liquid densities. The numerical solution of the governing equations shows that the sound wave propagation, the interfacial dynamics, and the flow field are properly described. The change of density at the interface has negligible effects on the structure of the solute field; as a consequence the trapping of solute is almost unaffected. On the other side, the slower interface dynamics induced by the flow field extends the stable branch of the $T_I(v_I)$ curve towards lower velocities. This reduces the region of the parameters' space where the oscillatory instability could be observed.

[1] M.C. Flemings, *Solidification Processing* (McGraw-Hill, New York, 1974).
[2] W. Kurz and D.J. Fisher, *Fundamentals of Solidification* (Trans Tech, Aedermannsdorf, 1992).
[3] G. Horvay, Int. J. Heat Mass Transf. **8**, 195 (1965).
[4] Ch. Charach and I. Rubinstein, J. Appl. Phys. **71**, 1128 (1992).
[5] G. Caginalp, Arch. Ration. Mech. Anal. **92**, 205 (1986).
[6] G. Caginalp, Phys. Rev. A **39**, 5887 (1989).
[7] G. Caginalp and P. Fife, Phys. Rev. B **33**, 7792 (1986).
[8] O. Penrose and P.C. Fife, Physica D **43**, 44 (1990).
[9] S.L. Wang, R.F. Sekerka, A.A. Wheeler, B.T. Murray, S.R. Coriell, R.J. Braun, and G.B. McFadden, Physica D **69**, 189 (1993).
[10] G.B. McFadden, A.A. Wheeler, R.J. Braun, S.R. Coriell, and R.F. Sekerka, Phys. Rev. E **48**, 2016 (1993).
[11] H. Lowen, J. Bechhofer, and L. Tuckerman, Phys. Rev. A **45**, 2399 (1992).
[12] A.A. Wheeler, B.T. Murray, and R.J. Schaefer, Physica D **66**, 243 (1993).
[13] G. Caginalp and J. Jones, Ann. Phys. (N.Y.) **237**, 66 (1995).
[14] G. Caginalp and W. Xie, Phys. Rev. E **48**, 1897 (1993).
[15] A.A. Wheeler, W.J. Boettinger, and G.B. McFadden, Phys. Rev. E **47**, 1893 (1993).
[16] M. Conti, Phys. Rev. E **56**, 3197 (1997).
[17] N.A. Ahmad, A.A. Wheeler, W.J. Boettinger, and G.B. McFadden, Phys. Rev. E **58**, 3436 (1998).
[18] Zhiqiang Bi and Robert F. Sekerka, Physica A **261**, 95 (1998).
[19] M. Conti, Phys. Rev. E **58**, 2071 (1998).
[20] M. Conti, Phys. Rev. E **58**, 6101 (1998).
[21] M. Conti and U. Marconi, Phys. Rev. E **63**, 011502 (2000).
[22] G. Caginalp and J. Jones, Appl. Math. Lett. **4**, 97 (1991).
[23] G. Caginalp and J. Jones, in *IMA Volumes on Mathematics and its Applications*, edited by M.E. Gurtin and G.B. McFadden (Springer, Berlin, 1991), pp. 29–50.
[24] D.W. Oxtoby and P.R. Harrowell, J. Chem. Phys. **96**, 3834 (1992).
[25] D.M. Anderson, G.B. McFadden, and A.A. Wheeler, Physica D **135**, 175 (2000).
[26] D.M. Anderson, G.B. McFadden, and A.A. Wheeler, Physica D **151**, 305 (2001).
[27] M. Conti, Phys. Rev. E **64**, 051601 (2001).
[28] R.F. Sekerka (unpublished).
[29] R. Evans, Adv. Phys. **28**, 143 (1979).
[30] A.J.M. Yang, P.D. Fleming III, and J.H. Gibbs, J. Chem. Phys. **64**, 3732 (1976).

[31] Ch. Charach and P.C. Fife, Open Syst. Inf. Dyn. **5**, 99 (1998).
[32] J.A. Warren and W.J. Boettinger, Acta Metall. Mater. **43**, 689 (1995).
[33] B. Caroli, C. Caroli, and B. Roulet, in *Solids Far From Equilibrium*, edited by Godreche (Cambridge University Press, Cambridge, 1992).
[34] M.J. Aziz and T. Kaplan, Acta Metall. **36**, 2335 (1988).
[35] M.J. Aziz and W.J. Boettinger, Acta Metall. Mater. **42**, 527 (1994).